Rift kinematics preserved in deep-time erosional landscape below the northern North Sea

Thilo Wrona[1,2]*, Alex Whittaker[3], Rebecca E. Bell[3], Robert L. Gawthorpe[1], Haakon Fossen[4], Christopher A-L. Jackson[5] and Marit Stokke Bauck[6,7]

[1]Department of Earth Science, University of Bergen, Allégaten 41, N-5007 Bergen, Norway

[2]GFZ German Research Centre for Geosciences, Telegrafenberg, 14473 Potsdam, Germany

[3]Department of Earth Science and Engineering, Imperial College, Prince Consort Road, London, SW7 2BP, UK

[4]Museum of Natural History, University of Bergen, Allégaten 41, N-5007, Bergen, Norway

[5]Department of Earth and Environmental Sciences, The University of Manchester, Williamson Building, Oxford Road, Manchester, M13 9PL, UK

[6]CGG, Lilleakerveien 6A, P.O.Box 43 Lilleaker, 0216 Oslo

[7]Department of Geosciences, University of Oslo, P.O. Box 1047 Blindern, N-0316 Oslo, Norway

ABSTRACT

Our understanding of continental rifting is, in large parts, derived from the stratigraphic record. This record is, however, incomplete as it does not often capture the geomorphic and erosional signal of rifting. New 3D seismic reflection data reveals a Late Permian-Early Triassic landscape incised into the pre-rift basement of the northern North Sea. This landscape, which covers at least 542 km^2, preserves a drainage system bound by two major tectonic faults. A

quantitative geomorphic analysis of the drainage system reveals 68 catchments, with channel steepness and knickpoint analysis of catchment-hosted palaeo-rivers showing that the landscape preserved a >2 Myrs long period of transient tectonics. We interpret that this landscape records punctuated uplift of the footwall of a major rift-related normal fault (Vette Fault) at the onset of rifting. The landscape was preserved by a combination of relatively rapid subsidence in the hangingwall of a younger fault (Øygarden Fault) and burial by post-incision sediments. We show how and why erosional landscapes are preserved in the stratigraphic record, and how they can help us understand the tectono-stratigraphic evolution of ancient continental rifts.

INTRODUCTION

Tectonics, landscape evolution, and strata are closely coupled in active continental rifts (e.g. Cowie et al., 2000; Gawthorpe and Leeder, 2000). Growing normal faults influence the geometry of drainage networks and incision rates within upland catchments, which in turn controls the location, magnitude, and routing of sediment supply to neighbouring depocenters (Cowie et al., 2006; Whittaker et al., 2010). This coupling means that the transient erosional response of fluvial landscapes to rifting can be used to record the timescales, throw rates and kinematics of active faulting over a range of spatial scales (e.g. Kirby and Whipple, 2012; Whittaker and Boulton, 2012). In modern rifts, we can analyse digital elevation models (DEMs), together with independent tectonic and stratigraphic constraints, to estimate the patterns and rates of fault evolution (e.g. Pechlivanidou et al., 2018; Watkins et al., 2020; Quye-Sawyer et al., 2021), but in many ancient rifts, similar rift-related palaeo-landscapes are absent. Consequently,

time-averaged patterns of faulting must be reconstructed indirectly from structural measurements and stratigraphic observations (e.g. Gawthorpe and Leeder, 2000, Kent et al., 2017). If palaeo-landscapes can be found in the stratigraphic record of ancient rifts, they may reveal important new information about fault behaviour.

To our knowledge, the oldest reported 3-D buried palaeo-landscapes are 55-58 Ma seismically imaged drainage networks found of the coast off Scotland, UK, developed and preserved in response to Iceland plume-driven uplift and subsidence (Hartley et al., 2011; Stucky de Quay et al., 2017). Here, we present an even older mountainous landscape, defined by an erosional surface carved into the Palaeozoic basement of the northern North Sea rift, offshore Norway, imaged in 3D seismic reflection data. The surface covers at least 542 km^2 and reveals a drainage system that developed at the onset of Permian-Triassic rifting (~261±10 Ma; Fossen & Dunlap, 1999). A quantitative geomorphic analysis of the surface shows that this drainage system contains an exceptional record of the transient landscape response to incipient faulting, from which we deduce the history and timescales of rift-related normal faulting. Our work shows how palaeo-surfaces imaged in 3D seismic reflection data can provide crucial insights into the tectono-stratigraphic evolution of ancient continental rifts.

GEOLOGICAL SETTING

The study area is located in the northern North Sea rift, offshore Norway (Fig. 1A). An up to 12 km thick syn- and post-rift sedimentary succession was deposited on crystalline basement during and after Late Permian-Early Triassic and Middle Jurassic-Early Cretaceous

rifting (Færseth, 1996; Bell et al., 2014; Maystrenko et al., 2017). In the Late Permian-Early Triassic, E-W extension led to the development of large (>100 km long) normal faults, such as the W-dipping Tusse, Vette and Øygarden faults, which bound half-grabens and are the focus of this study (Fig. 1A,B). By the Triassic, these faults had developed large displacements (up to 4 km) and were associated with relatively high slip rates (0.1–0.15 mm/yr; Bell et al., 2014); however, the relative age of these faults remains unknown. The top of the basement in the footwall of the Vette Fault is capped by a distinct erosional surface (Fig. 1B), which we describe and analyse below. From seismic and well data, we know that the surface is capped by upper Permian and Lower Triassic succession composed of alluvial and fluvial rocks (Evans, 2003).

METHODS

3D seismic reflection data

Acquisition

The seismic data (courtesy of CGG) used in this study were acquired with a G-Gun array consisting of 3 subarrays with a source array depth of 6-9 m; a source length of 16-18 m; a shot point interval of 18.75 m; source separation of 37.5 m; a volume of 0.07456 m^3 and an air pressure of $1.379 \cdot 10^7$ Pa. The streamer consisted of 12 up to 8 km long cables with 636 channels each; a cable separation of 75 m and group spacing of 12.5 m; depths of 7-50 m covering offsets of 150-8100 m. The data was recorded with a 2 ms sample interval; 9000 ms recording length; a low cut filter (2Hz-6db/oct) and high cut (200 Hz-370 db/oct) filter.

Processing

The seismic data were processed in 90 steps including: divergence compensation; low cut filter (1.5 Hz, 2.5 Hz); noise attenuation (e.g. swell, direct wave); spatial anti-aliasing filter (12.5 m group interval); direct wave attenuation; source de-signature; de-spike; time-variant high cut filter; receiver motion correction and de-ghosting; FK filter; cold water and tidal statics; multiple modelling with adaptive subtraction; Tau-P mute; Radon de-multiple; far angle destriping; multiple attenuation; binning (75 m interval, 107 offset planes); acquisition hole infill; 5-D regularization; 3-D true amplitude Kirchhoff pre-stack depth migration; residual move-out correction; Linear FL Radon; full offset stack with time-variant inner and out mute; acquisition footprint removal; crossline K filter; residual de-striping and dynamic Q-compensation. The seismic volume was zero phase processed with SEG normal polarity.

Seismic interpretation

We use broadband 3D seismic reflection data to map the top of the acoustic basement at a spatial resolution (i.e. bin size) of 12.5×18.5 m revealing a palaeo-landscape preserved in the footwall of the Vette Fault (Fig. 1). The top of the acoustic basement is a high-amplitude reflection originating from the impedance contrast between sedimentary rocks (above) and crystalline basement (below). We also map two seismically distinct, wedge-shaped Permian-Triassic units to understand the preservation of the landscape (Unit 1 showing medium-to-low amplitude, sub-horizontal layering and Unit 2; characterised by chaotic, discontinuous low amplitudes (e.g. Fig. 1B).

Surface restoration

To analyse the geomorphology of this surface, we create a DEM by restoring the seismic horizon to its original geometry (cf. Hartley et al., 2011; Stucky de Quay et al., 2017) (Fig. 2). First, we map the basement surface (Fig. 2A, B) and the first continuous onlap horizon overlying the surface (Fig. 2C, D). As this horizon shows almost no topography, we can obtain original surface morphology by flattening the basement surface using the onlap horizon (Fig. 2E, F). Then, we rotate the surface by 3° to the West to remove the effect of eastward fault block rotation during subsequent rifting (Fig. 3D). Note that 3° rotation results in a realistic stream network (Fig. 3). Finally, we grid the restored basement surface, so it becomes a digital elevation model (DEM) with a cell size of 50×50 m.

Geomorphic analysis

Network extraction

We performed a quantitative analysis of the restored DEM using TopoToolbox 2 (Schwanghart and Scherler, 2014) and recovered stream networks and river long profiles using a D8 flow routing algorithm with a flow accumulation threshold of 0.25 km^2 typically used in modern systems (e.g. Whittaker and Boulton, 2012) (Fig. 4E). This threshold corresponds to the minimum area draining into one cell belonging to a river. If this value is too low, we introduce an unrealistically large number of first-order tributaries (Fig. 4A-C). As the derivation of a stream network requires a consistent hydrological surface, pits in the reconstructed DEM must be filled. To remove any erroneous elevation values, we use the seismic resolution (18 m i.e. quarter of the wavelength) as the maximum filling depth of the DEM (Fig. 5B). Our ancillary analysis of filling

depth sensitivity shows that when this value is too high, river networks are straightened and begin to show unrealistic geometries (Fig. 5D, E).

Channel steepness calculation

River incision upstream of active fault is often well-described by a family of stream power erosion 'laws' (Tucker and Whipple, 2002; Whittaker et al., 2007; Kirby and Whipple, 2012; Whittaker and Walker, 2015). In these cases, channel slope (S) is related to the upstream drainage area (A) by a power law, which would imply that rivers in topographic steady-state exhibit a concave up profile that represents a balance between a downstream increase in discharge and the downstream decrease in channel gradient. For a classic stream power model, we can write:

$$S = \left(\frac{U}{K}\right)^{\frac{1}{n}} A^{\frac{-m}{n}} \quad (1)$$

where U represents an uplift rate (for example driven by faulting), K is a coefficient that includes bedrock erodibility and other factors, and m and n are positive exponents which related to both the long term erosional dynamics of the system and its hydraulic geometry (e.g. Kirby and Whipple, 2012). The term $\left(\frac{U}{K}\right)^{\frac{1}{n}}$ is known as the channel steepness index, ks, and the ratio of m/n by the channel concavity, θ. A reference value of θ is often used to estimate a normalized channel steepness index, ksn, allowing comparisons between channels with different concavities (e.g. Snyder et al., 2000; Wobus et al., 2006). In this study, we assume that n is 1 to calculate our steepness index, as this is consistent with previous studies of rivers crossing normal faults (e.g.

Whittaker and Boulton, 2012; Roda-Boluda and Whittaker, 2017). Using a global mean concavity index for channels of 0.45 (Schwanghart and Scherler, 2014), we calculate normalized channel steepness along our network.

Knickpoint extraction

Knickpoints upstream of active faults reflect the transient response of fluvial systems to relative base level change (such as a change in fault slip rate). The reach downstream of a knickpoint has steepened and incised in response to the perturbation, while upstream has yet to respond geomorphically to the uplift event, and retains its pre-existing configuration (Kirby and Whipple, 2012). Knickpoints migrate upstream over time, eventually transmitting the initial perturbation throughout the catchment area over timescales of 10^6 years or more (Tucker and Whipple, 2002; Harkins et al., 2007; Whittaker et al., 2010). We identify knickpoints in the palaeo-river long profiles of our stream network using the TopoToolbox 2 (Schwanghart and Scherler, 2017). The knickpoint finder reconstructs to the actual longitudinal profile by iteratively removing a curvature constraint at those locations that have a maximum vertical offset to the profile. After a few iterations, the vertical offset decreases to a minimum tolerance set by the user (Figs. 6, 7). Because this tolerance should reflect uncertainty in the data (Schwanghart and Scherler, 2017), we use 2.5 times the seismic resolution of our survey (45 m). This high tolerance assures that we extract only major knickpoints in the network (Figs. 6, 7, 8C, D).

After the extraction, we measure the elevation of these knickpoints relative to the Vette Fault (where it cuts the river) to a precision of ± 25 m, and their distance upstream with a

precision of ± 100 m (Tab. 1). Knickpoint height relative to the fault is compared to geologic constraints on fault throw (cf. Bell et al., 2014) and knickpoint locations are compared to palaeo-catchment drainage area (Fig. 9).

Migration time estimation

For any knickpoints located upstream of the footwall-bounding Vette Fault, we estimate a potential timescale for their propagation upstream, assuming they started from the fault, using an estimated propagation velocity V, derived from a unit stream power erosion law (Tucker and Whipple, 2002; Whittaker et al., 2012) given by $V = K \cdot A^{0.5}$, where K is a parameter that relates to a number of factors including bedrock strength and A is the drainage area of the catchment (e.g. Whittaker et al., 2008). This means that migration rates decrease as knickpoints migrate upstream and upstream drainage areas reduce (e.g. Whittaker et al., 2008). In our case, we can capture this effect by computing the upstream drainage area of each knickpoint for each time-step. Next we estimate knickpoint migration times by stepwise summation of the product of the migration distance, the drainage-area normalized migration rate, and the upstream drainage area. We use $K = 5.0 \cdot 10^{-7}$ per year based on the average of a well-constrained compilation of modern systems upstream of active faults with similar drainage areas and slip rates < 0.5 mm/yr (Whittaker and Boulton, 2012) (Fig. 10).

RESULTS

Seismic and geomorphic expression of the palaeo-landscape

Our study area covers an area of ~542 km^2 and is located between the Vette and the Øygarden faults (Fig. 1). The surface is carved into ‘basement’ rocks, which are likely to consist

of Devonian sedimentary rocks, Caledonian allochthons, and Proterozoic crystalline rocks based on the onshore geology (Fazlikhani et al., 2017). In cross-section, the surface is highly irregular, showing relatively steep slopes (up to 15°) and moderate relief (<800 m) (Fig. 1B). This seismically defined morphology, combined with our subsequent geomorphic analysis (Fig. 2) and the depositional setting of the overlying, non-marine Triassic deposits (Evans, 2003) filling and preserving the unconformity surface, are very strong evidence that the surface represents a subaerial landscape.

Our DEM analysis of the surface reveals an intricate 3D landscape showing a small fault-bounded mountain range with relief up to 800 m, incised by a dendritic fluvial network, from which individual catchments can be identified with exceptional clarity (Fig. 2A). Consequently, our results depict a unique "snapshot" of an ancient footwall landscape, which based on the seismic stratigraphy must have formed during footwall uplift in response to slip accumulation on the Vette Fault (Fig. 1B).

Landscape response to active faulting at 250 Ma

From this unique palaeo-landscape, we extracted 68 palaeo-catchments with drainage areas up to 60 km^2 from the DEM (Tab. 1). The longest trunk rivers are up to 20 km long. Many catchments show abrupt channel steepness index variations (Fig. 8B). For instance, high steepness index river segments (>50 m long) are mainly found in catchments that decrease in elevation and appear to drain westwards towards the Vette Fault, (Fig. 8B). Reconstructed palaeo-channel long profiles are *not* concave up, but show distinct convexities on a range of

length scales (Fig. 8D). The channel geometries are remarkably similar to those observed in modern fluvial systems draining across active normal faults (cf. Whittaker, 2012). Consequently the sharp variations in channel steepness suggest that the palaeo-landscape was not in a topographic steady state when preserved.

We extract 28 knickpoints from the palaeo-river long profiles (Fig. 8C, D; Tab. 2). Thirteen catchments have at least one significant knickpoint upstream of the Vette Fault and several have two. These knickpoints lie at distances between 0.44-10 km upstream of the Vette Fault, with elevations for the lower or single set of knickpoints varying between 45->300 m (Fig. 10). In terms of their size and scale, these catchments and knickpoints are comparable to modern fluvial systems crossing faults in Italy, Turkey, and Greece (Whittaker and Boulton, 2012; Whittaker and Walker, 2015; Roda-Boluda and Whittaker, 2017) (Fig. 9), where rivers have been shown to record changing fault slip rates over timescales of 1-5 million years.

When plotted along the strike of the Vette Fault, elevation of the knickpoints relative to the fault is an order of magnitude smaller than the fault throw between 0-40 km along strike, with these values being comparable for the northern part of the fault (Fig. 10). Knickpoint elevations are smallest 25-40 km along strike, which is where throw is presently greatest (Fig. 10B,C). Given that knickpoint elevation, since formation, scales predictably with fault slip rate (cf. Whittaker and Walker, 2015), we infer that along-strike changes in elevation define two palaeo fault segments that were active early in the evolution of the Vette Fault. The upper set of knickpoints also have elevations that are considerably less than the geologic throw. Although

there is some scatter, single knickpoints on palaeo-catchments with bigger drainage areas are located predictably further upstream, ($L \sim A^{0.38\pm0.12}$) (Fig. 9) which is consistent with them forming at a similar time. Consequently, we interpret these knickpoints to capture the transient response of the footwall landscape to the early growth of the Vette Fault near the onset of Permian-Triassic rifting. The palaeo-landscape was subsequently buried in the hanging wall of the Øygarden Fault before the transient tectonic signal had a chance to propagate fully through the fluvial system.

DISCUSSION

Preserved landscape – transient tectonics

Our study reveals a subaerial drainage system carved into the footwall of the Vette Fault, northern North Sea Rift (Fig. 1). The overlying stratigraphy indicates that this landscape developed during Permian-Triassic rifting (Bell et al., 2014). Our geomorphic analysis of the system reveals that many catchments draining across the Vette Fault have high (>60) steepness indices (Fig. 8B), and that 13 of the 68 catchments have knickpoints, which are indicative of an increase in tectonic uplift rates (Fig. 8C) (*sensu* Hartley et al., 2011; Stucky de Quay et al., 2017). The seismically imaged palaeo-rivers thus capture the landscape response to footwall uplift, generated by growth of the Vette Fault around 250 Ma. The presence of two sets of knickpoints suggests more than one change in fault slip rates during the early evolution of the fault. This likely reflects throw rate increases driven by fault growth and perhaps linkage,

evidenced by the fact that the lower set of knickpoints appears to record two, presumably unlinked, palaeo segments.

Duration of faulting and knickpoint migration

Once formed, tectonically-driven knickpoints migrate upstream, as catchments progressively respond to the relative change in base level (Kirby and Whipple, 2012). We can thus use the duration of knickpoint migration upstream of the Vette Fault as a proxy for the time of fault activity. Knickpoint elevation upstream of interacting fault segments is known to scale with the relative difference in throw rates and the time since this has taken place (Whittaker & Boulton, 2012). The maximum elevation of the lower knickpoints is ~250 m. If we divide this by published time-averaged throw rates on the Vette Fault of 0.15 mm/yr (Bell et al., 2014) as a maximum, this would imply that the transient landscape represents a minimum of 1.7 Myrs, similar to faulted landscapes in Greece (e.g. Whittaker and Walker, 2015). Alternatively, if we calculate upstream migration of the knickpoints using bedrock erodibilities based on an average of a compilation of modern systems upstream of active faults with similar drainage areas and slip rates, we obtain a preferred median landscape response time of 2.1 Myrs and extremes of a 1.1 to 10.1 Myrs; this suggests that the palaeo-landscape records fault growth and interaction over periods of a few million years (Fig. 4C). Considering that dating of sedimentary rocks, fault rocks, and dykes suggest that Permian-Triassic rifting began around 261±10 (Fossen & Dunlap, 1999) and lasted tens of millions of years (Ravnås et al., 2000; Fossen et al., 2021), our results indicate that the Vette Fault was only this active for a fraction of this episode.

Landscape preservation – strain migration

To understand the preservation of this landscape, we reconstruct the tectono-stratigraphic context and evolution of the system through time (Fig. 11). The landscape developed at the onset of rifting in the northern North Sea, when the young Vette Fault initiated, and when Permian-Triassic strata (Unit 1) were being deposited in its immediate hanging wall (Fig. 4A). The knickpoints and overall landscape were created when segments of the Vette Fault were displacing palaeo-streams and rivers (Fig. 2C). Subsequently, the drainage system was rapidly buried and preserved beneath Permian-Triassic strata (Unit 2) (Figs. 1B, 4B). The rapid burial of the footwall of the Vette Fault, before the transient landscape had equilibrated, was likely driven by strain migration from the Vette Fault to the Øygarden Fault, with the hanging wall of the former producing subsidence that outpaced footwall uplift on the Vette Fault.

CONCLUSIONS

This study reveals a subaerial drainage system carved into the basement surface of the northern North Sea Rift. This system covers at least 542 km^2 and is bound by two major tectonic faults. A quantitative geomorphic analysis of the drainage system reveals 68 catchments, with channel steepness and knickpoint analysis of catchment-hosted palaeo-rivers showing that the landscape preserved a >2 Myrs long period of transient tectonics driven by fault growth and interaction. We interpret that this landscape records punctuated uplift of the footwall of a major rift-related normal fault at the onset of rifting.

ACKNOWLEDGMENTS

The project received financial support from The Norwegian Academy of Science and Letters (VISTA), The University of Bergen and The Initiative and Networking Fund of the Helmholtz Association through the project "Advanced Earth System Modelling Capacity (ESM) and The Geo.X The Research Network for Geoscience in Berlin and Potsdam. Furthermore, we thank CGG for the permission to publish this data and Leo Zijerveld for IT support.

REFERENCES CITED

Bell, R. E., Jackson, C. A. L., Whipp, P. S., & Clements, B. (2014). Strain migration during multiphase extension: Observations from the northern North Sea. *Tectonics*, *33*(10), 1936–1963. https://doi.org/10.1002/2014TC003551

Cowie, P. A., Attal, M., Tucker, G. E., Whittaker, A. C., Naylor, M., Ganas, A., & Roberts, G. P. (2006). Investigating the surface process response to fault interaction and linkage using a numerical modelling approach. *Basin Research*, *18*(3), 231–266. https://doi.org/10.1111/j.1365-2117.2006.00298.x

Cowie, P. A., Gupta, S., & Dawers, N. H. (2000). Implications of fault array evolution for synrift depocentre development: insights from a numerical fault growth model. *Basin Research*, *12*(3–4), 241–261. https://doi.org/10.1046/j.1365-2117.2000.00126.x

Evans, D. (2003). *The Millennium Atlas: Petroleum Geology of the Central and Northern North Sea;[a Project of the Geological Society of London, the Geological Survey of Denmark and Greenland and the Norwegian Petroleum Society]*.

Færseth, R. B. (1996). Interaction of permo-triassic and jurassic extensional fault-blocks during the development of the northern North Sea. *Journal of the Geological Society*, *153*(6), 931–944. https://doi.org/10.1144/gsjgs.153.6.0931

Fazlikhani, H., Fossen, H., Gawthorpe, R. L., Faleide, J. I., & Bell, R. E. (2017). Basement structure and its influence on the structural configuration of the northern North Sea rift. *Tectonics*, *36*(6), 1151–1177. https://doi.org/10.1002/2017TC004514

Fossen, H., & Dunlap, W. J. (1999). On the age and tectonic significance of Permo-Triassic dikes in the Bergen-Sunnhordland region, southwestern Norway. *Norsk Geologisk Tidsskrift*, *79*(3), 169–177. https://doi.org/10.1080/002919699433807

Fossen, H., Ksienzyk, A. K., Rotevatn, A., Bauck, M. S., & Wemmer, K. (2021). From widespread faulting to localised rifting: Evidence from K‐Ar fault gouge dates from the Norwegian North Sea rift shoulder. *Basin Research*, 33, 1934-1953. doi:10.1111/bre.12541

Gawthorpe, R. L., & Leeder, M. R. (2000). Tectono-sedimentary evolution of active extensional basins. *Basin Research*, *12*(3–4), 195–218. https://doi.org/DOI 10.1046/j.1365-2117.2000.00121.x

Harkins, N., Kirby, E., Heimsath, A., Robinson, R., & Reiser, U. (2007). Transient fluvial incision in the headwaters of the Yellow River, northeastern Tibet, China. *Journal of Geophysical Research: Earth Surface*, *112*(3). https://doi.org/10.1029/2006JF000570

Hartley, R. A., Roberts, G. G., White, N., & Richardson, C. (2011). Transient convective uplift of an ancient buried landscape. *Nature Geoscience*, *4*(8), 562–565. https://doi.org/10.1038/ngeo1191

Kent, E., Boulton, S. J., Whittaker, A. C., Stewart, I. S., & Cihat Alçiçek, M. (2017). Normal fault growth and linkage in the Gediz (Alaşehir) Graben, Western Turkey, revealed by transient river long-profiles and slope-break knickpoints. *Earth Surface Processes and Landforms*, *42*(5), 836–852. https://doi.org/10.1002/esp.4049

Kirby, E., & Whipple, K. X. (2012). Expression of active tectonics in erosional landscapes. *Journal of Structural Geology*, *44*, 54–75. https://doi.org/10.1016/j.jsg.2012.07.009

Maystrenko, Y. P., Olesen, O., Ebbing, J., & Nasuti, A. (2017). Deep structure of the northern north sea and southwestern Norway based on 3D density and magnetic modelling. *Norsk Geologisk Tidsskrift*, *97*(3), 169–210. https://doi.org/10.17850/njg97-3-01

Pechlivanidou, S., Cowie, P. A., Hannisdal, B., Whittaker, A. C., Gawthorpe, R. L., Pennos, C., & Riiser, O. S. (2017). *Source-to-sink analysis in an active extensional setting: Holocene erosion and deposition in the Sperchios rift, central Greece*. https://doi.org/10.1111/bre.12263

Quye‐Sawyer, J., Whittaker, A. C., Roberts, G. G., & Rood, D. H. (2021). Fault Throw and Regional Uplift Histories From Drainage Analysis: Evolution of Southern Italy. *Tectonics*, *40*(4). https://doi.org/10.1029/2020tc006076

Ravnås, R., Nøttvedt, A., Steel, R. J., & Windelstad, J. (2000). Syn-rift sedimentary architectures in the Northern North Sea. *Geological Society Special Publication*, *167*, 133–177. https://doi.org/10.1144/GSL.SP.2000.167.01.07

Roda-Boluda, D. C., & Whittaker, A. C. (2017). Structural and geomorphological constraints on active normal faulting and landscape evolution in Calabria, Italy. *Journal of the Geological Society*, *174*(4), 701–720. https://doi.org/10.1144/jgs2016-097

Schwanghart, W., & Scherler, D. (2014). Short Communication: TopoToolbox 2 - MATLAB-based software for topographic analysis and modeling in Earth surface sciences. *Earth Surface Dynamics*, *2*(1), 1–7. https://doi.org/10.5194/esurf-2-1-2014

Schwanghart, Wolfgang, & Scherler, D. (2017). Bumps in river profiles: Uncertainty assessment and smoothing using quantile regression techniques. *Earth Surface Dynamics*, *5*(4), 821–839. https://doi.org/10.5194/esurf-5-821-2017

Snyder, N. P., Whipple, K. X., Tucker, G. E., & Merritts, D. J. (2000). Landscape response to tectonic forcing: Digital elevation model analysis of stream profiles in the Mendocino triple junction region, Northern California. *Bulletin of the Geological Society of America*, *112*(8), 1250–1263. https://doi.org/10.1130/0016-7606(2000)112<1250:LRTTFD>2.0.CO;2

Stucky de Quay, G., Roberts, G. G., Watson, J. S., & Jackson, C. A. L. (2017). Incipient mantle plume evolution: Constraints from ancient landscapes buried beneath the North Sea. *Geochemistry, Geophysics, Geosystems*, *18*(3), 973–993. https://doi.org/10.1002/2016GC006769

Tucker, G. E., & Whipple, K. X. (2002). Topographic outcomes predicted by stream erosion models: Sensitivity analysis and intermodel comparison. *Journal of Geophysical Research: Solid Earth*, *107*(B9), ETG 1-1-ETG 1-16. https://doi.org/10.1029/2001jb000162

Watkins, S. E., Whittaker, A. C., Bell, R. E., S Brooke, S. A., Ganti, V., Gawthorpe, R. L., McNeill, L. C., Nixon, C. W., & Stephen Watkins, C. E. (2020). Straight from the source's mouth: Controls on field-constrained sediment export across the entire active Corinth Rift, central Greece. *1600 | Basin Research*, *32*, 1600–1625. https://doi.org/10.1111/bre.12444

Whittaker, A. C., Attal, M., & Allen, P. A. (2010). Characterising the origin, nature and fate of sediment exported from catchments perturbed by active tectonics. *Basin Research*, *22*(6), 809–828. https://doi.org/10.1111/j.1365-2117.2009.00447.x

Whittaker, A. C., Attal, M., Cowie, P. A., Tucker, G. E., & Roberts, G. (2008). Decoding temporal and spatial patterns of fault uplift using transient river long profiles. *Geomorphology*, *100*(3–4), 506–526. https://doi.org/10.1016/j.geomorph.2008.01.018

Whittaker, A. C., & Boulton, S. J. (2012). Tectonic and climatic controls on knickpoint retreat rates and landscape response times. *Journal of Geophysical Research: Earth Surface*, *117*(2). https://doi.org/10.1029/2011JF002157

Whittaker, A. C., Cowie, P. A., Attal, M., Tucker, G. E., & Roberts, G. P. (2007). Bedrock channel adjustment to tectonic forcing: Implications for predicting river incision rates. *Geology*, *35*(2), 103–106. https://doi.org/10.1130/G23106A.1

Whittaker, A. C., & Walker, A. S. (2015). Geomorphic constraints on fault throw rates and linkage times: Examples from the Northern Gulf of Evia, Greece. *Journal of Geophysical Research F: Earth Surface*, *120*(1), 137–158. https://doi.org/10.1002/2014JF003318

Wobus, C., Whipple, K. X., Kirby, E., Snyder, N., Johnson, J., Spyropolou, K., Crosby, B., & Sheehan, D. (2006). Tectonics from topography: Procedures, promise, and pitfalls. *Special Paper of the Geological Society of America*, *398*, 55–74. https://doi.org/10.1130/2006.2398(04)

FIGURES

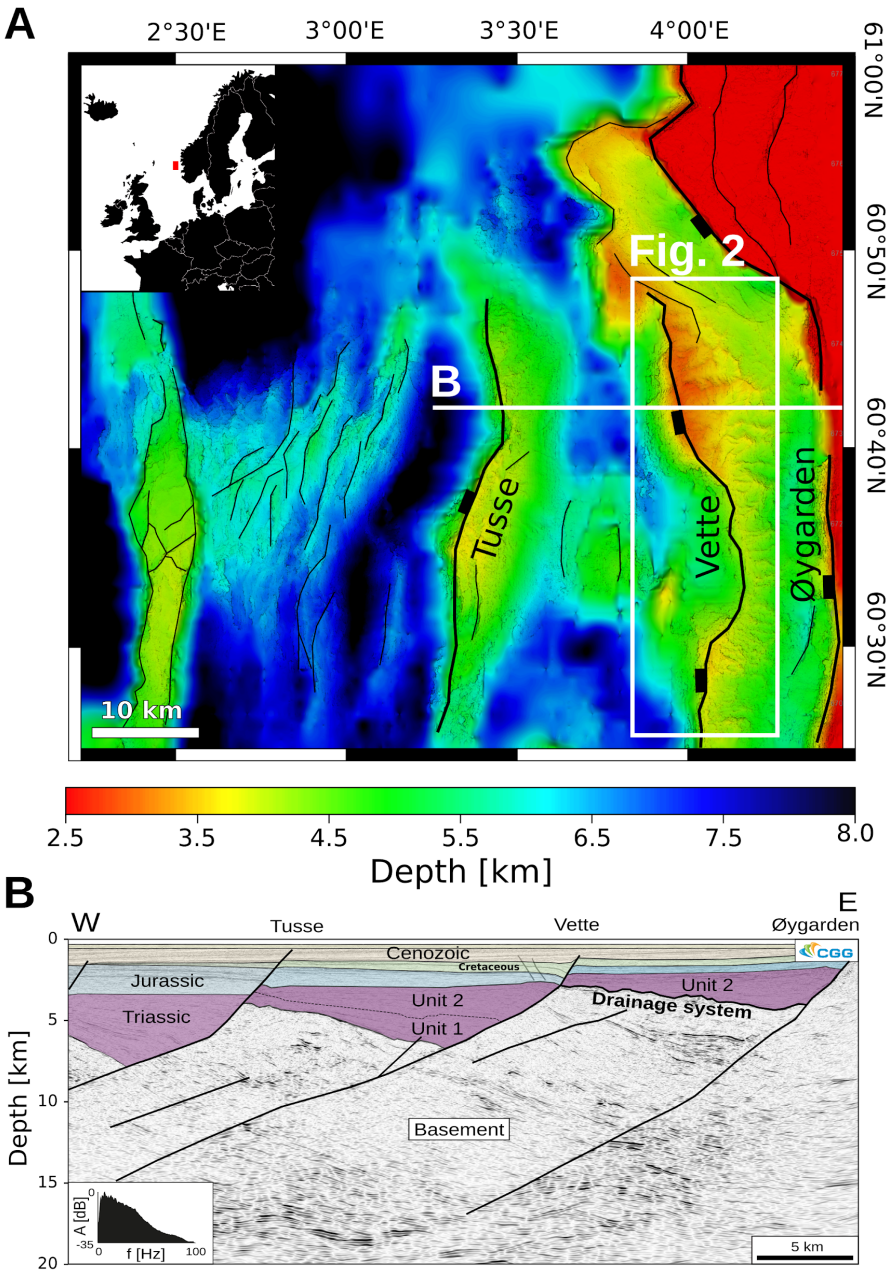

Figure 1. **A** Map view of the interpreted basement surface showing rift-related normal faults and drainage system in the northern North Sea. **B** Seismic section (depth-migrated) showing the drainage systems situated on top of the basement. Permian-Triassic strata overlying the surface consists of two wedge-shaped units Seismic data courtesy of CGG.

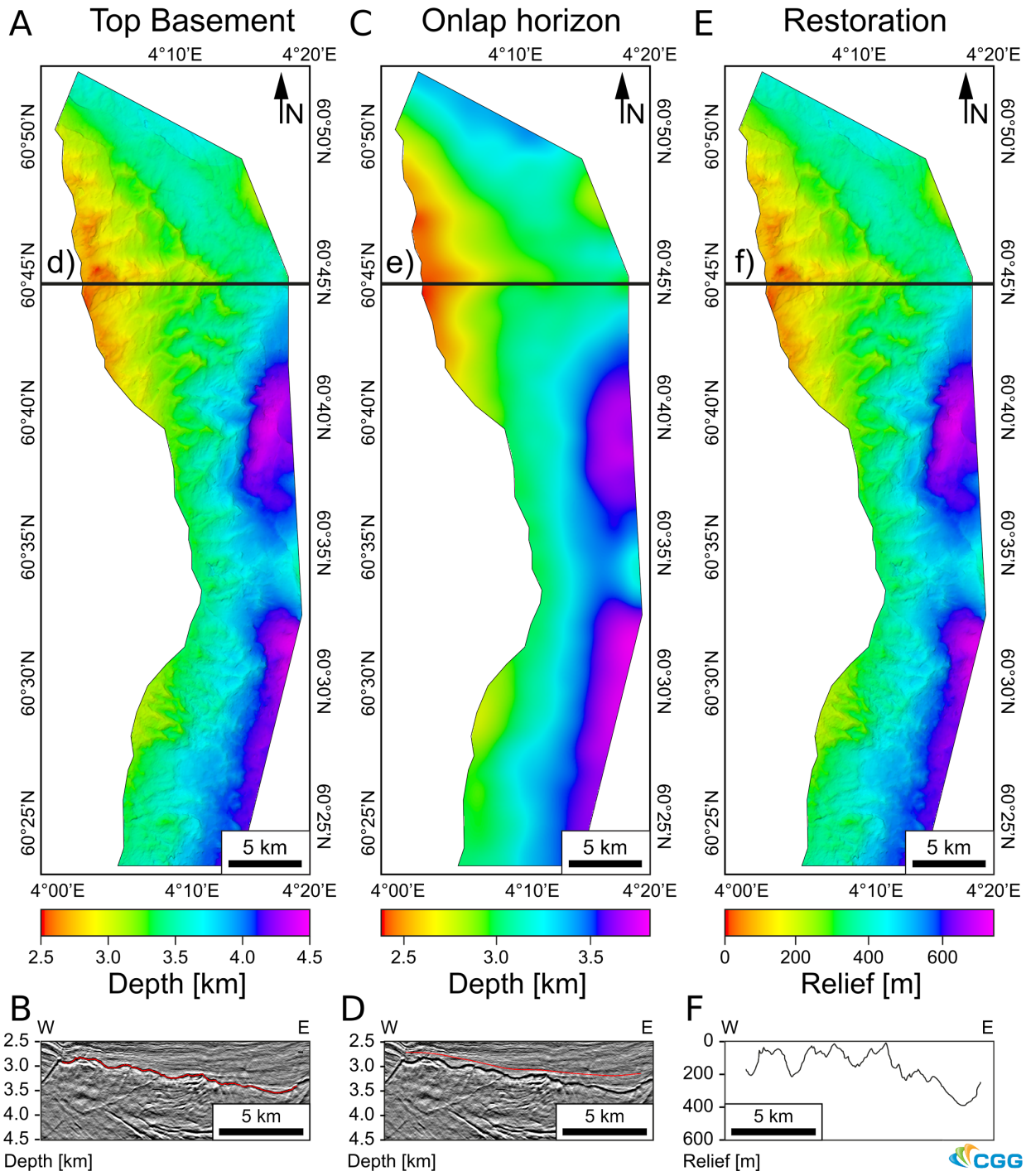

Figure 2. A Top Basement surface showing the drainage system. **B** Seismic section showing the surface interpretation. **C** Onlap horizon (smoothed). **D** Seismic section showing the horizon onlapping onto the Top Basement surface. **E** Top Basement surface flattened on the onlapping horizon to restore original morphology. **F** Profile of restored basement relief along seismic section. Seismic data courtesy CGG.

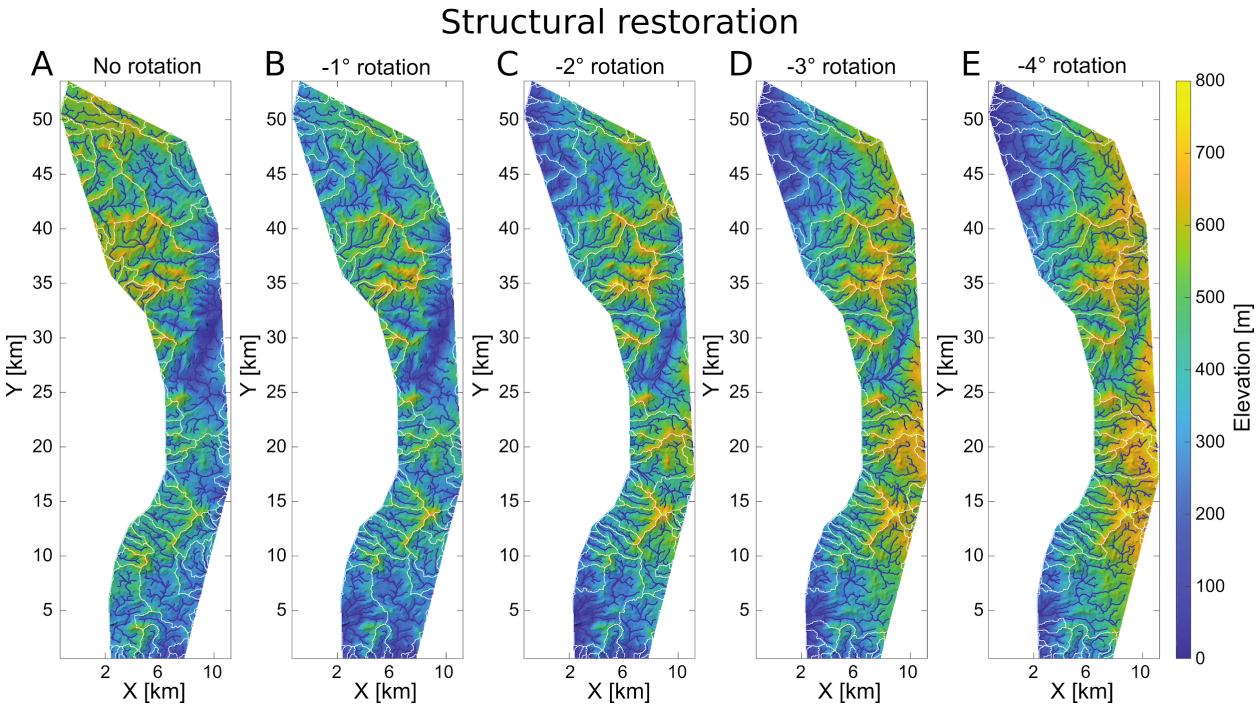

Figure 3. Basement surface with stream network and drainage divides restored for different degrees of fault block rotation (0-4°). A moderate rotation of 3° results in a realistic stream network (D).

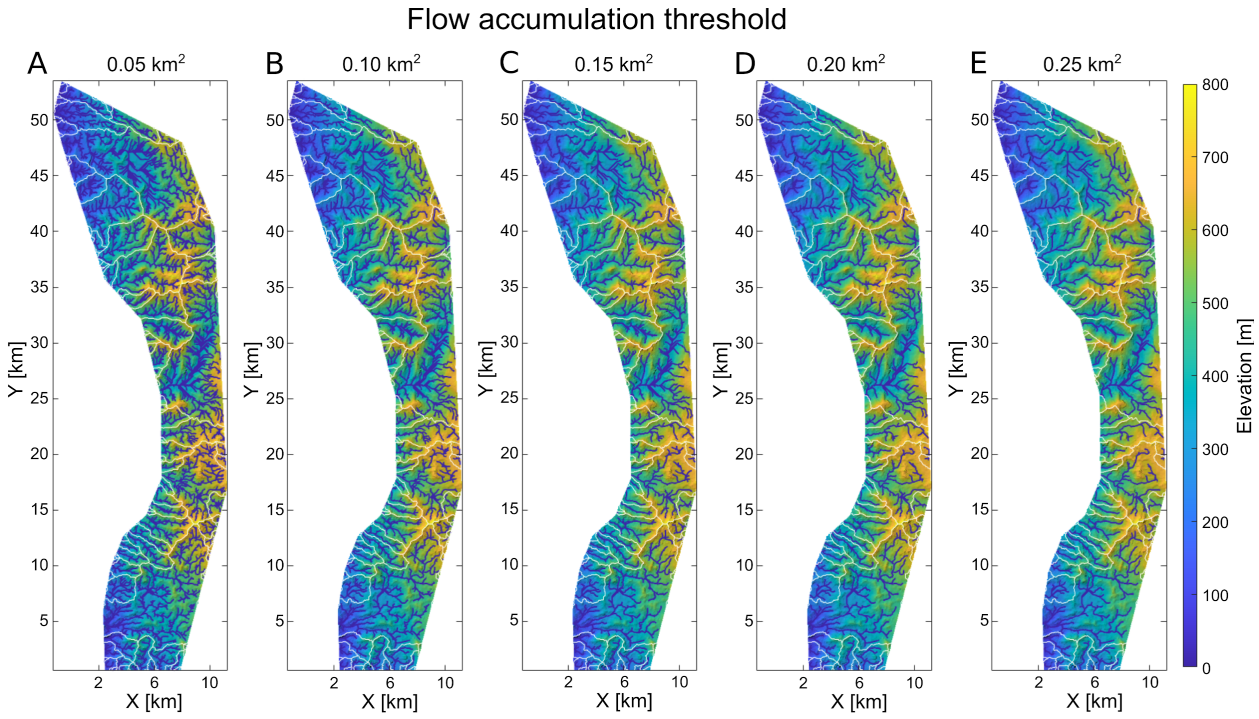

Figure 4. Basement surface with stream network and drainage divides for different flow accumulation cutoffs. Note that low cutoff values result in more tributaries. We chose a flow accumulation threshold of 0.25 km^2 (E) typically used in modern systems (e.g. Whittaker and Boulton, 2012).

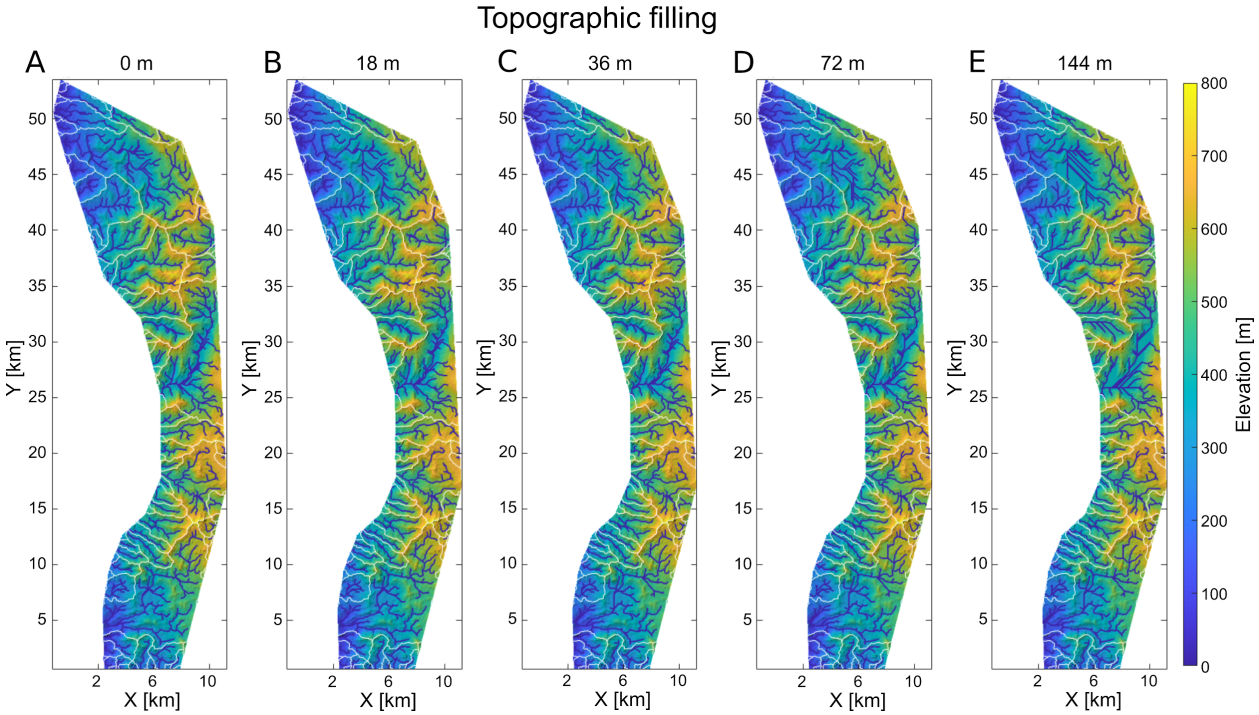

Figure 5. Basement surface with stream network and drainage divides for different amounts of topographic filling. Note that high filling values result in straightened streams and rivers. To remove erroneous elevation values, we use the seismic resolution of 18 m (B) as the maximum filling depth of the DEM.

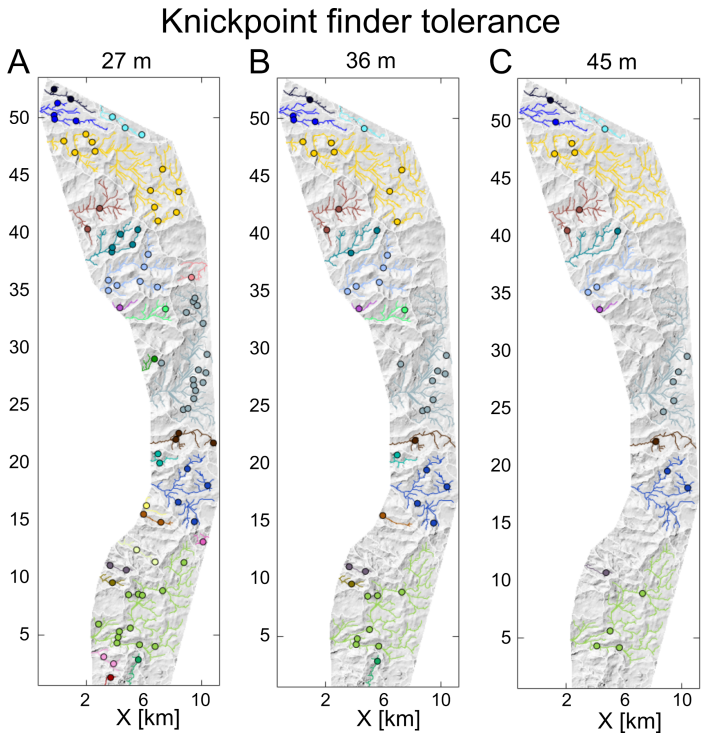

Figure 6. Knickpoints in map view extracted for different tolerance values of **A** 27, **B** 36 and **C** 45 m.

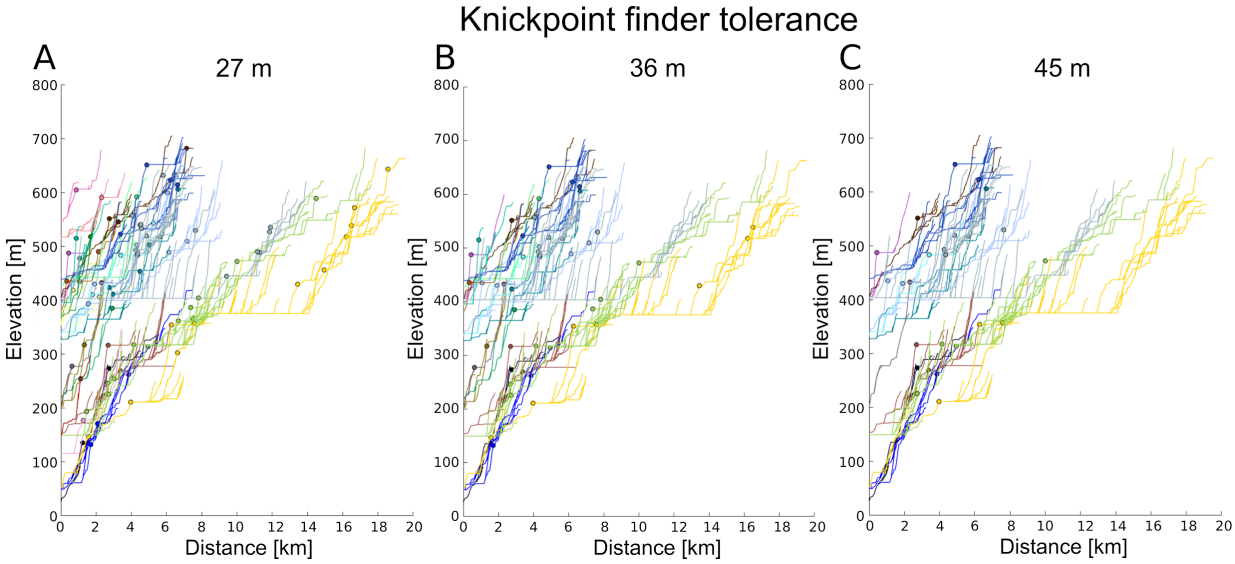

Figure 7. Knickpoints along elevation profiles extracted for different tolerance values of **A** 27, **B** 36 and **C** 45 m.

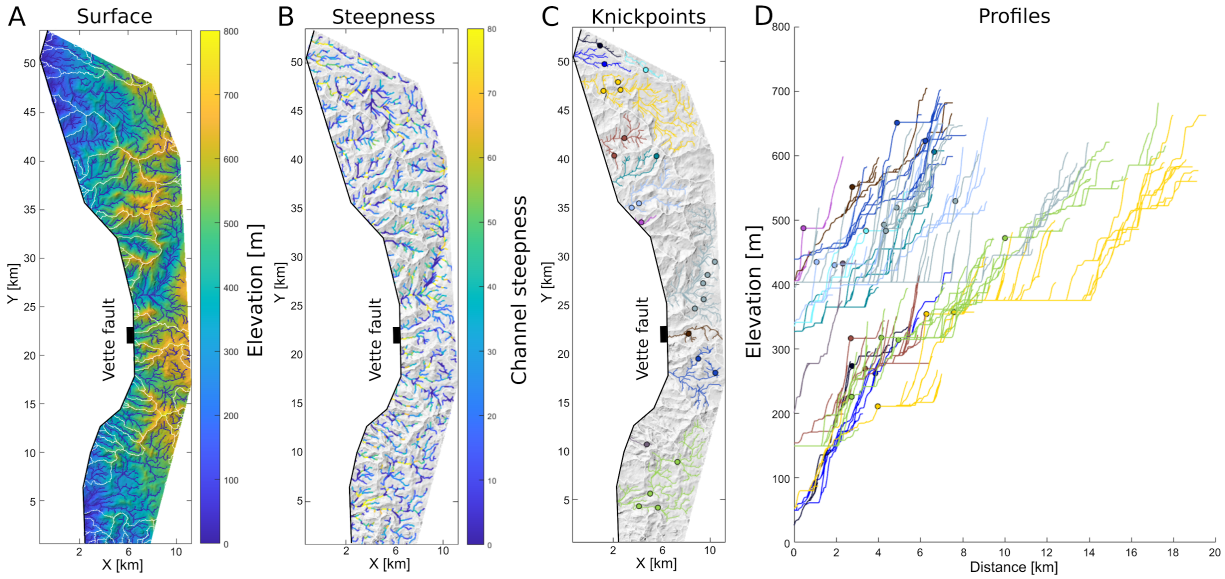

Figure 8. A Restored basement surface with stream network and drainage divides. **B** Normalized channel steepness index of stream network. **C** Knickpoints in map view extracted from stream network. **D** Knickpoints along profile extracted from stream network

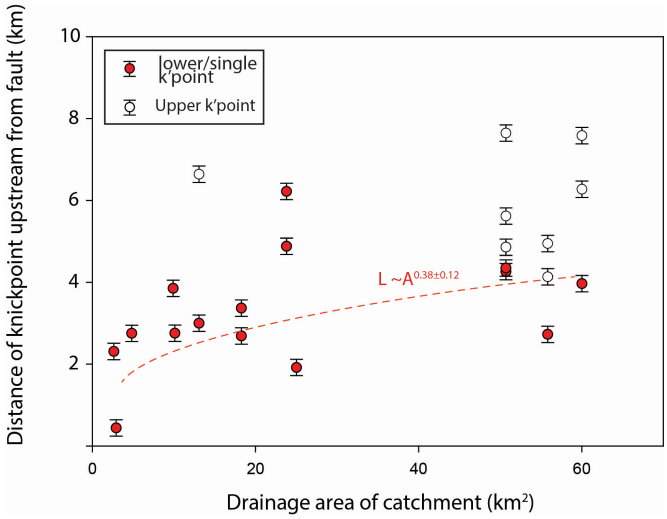

Figure 9. Upstream distance versus catchment plot.

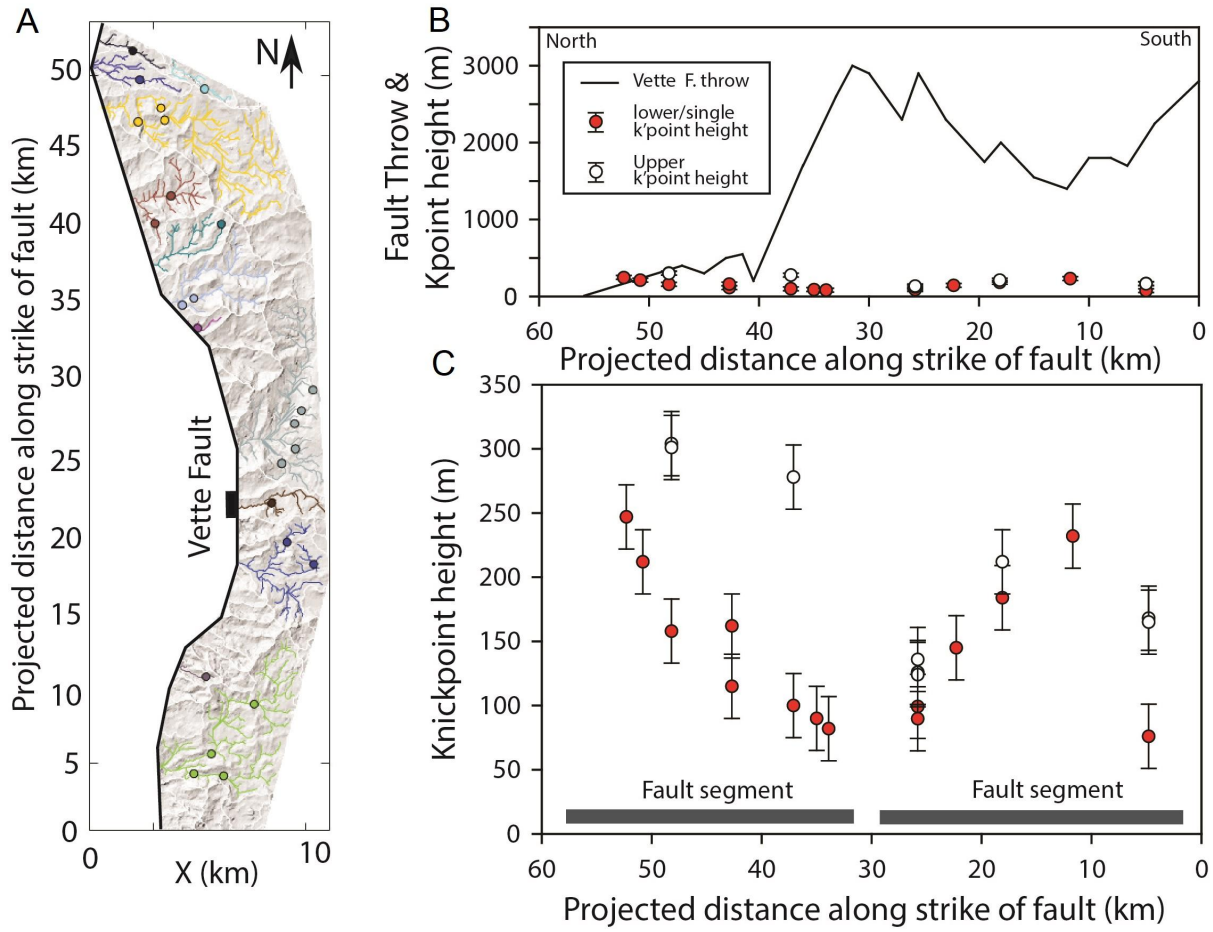

Figure 10: A Knickpoints extracted from stream network. **B** Knickpoint height and fault throw along strike (same scale). **C** Knickpoint height with error bar. Note the two populations of knickpoints (upper-white and lower-red).

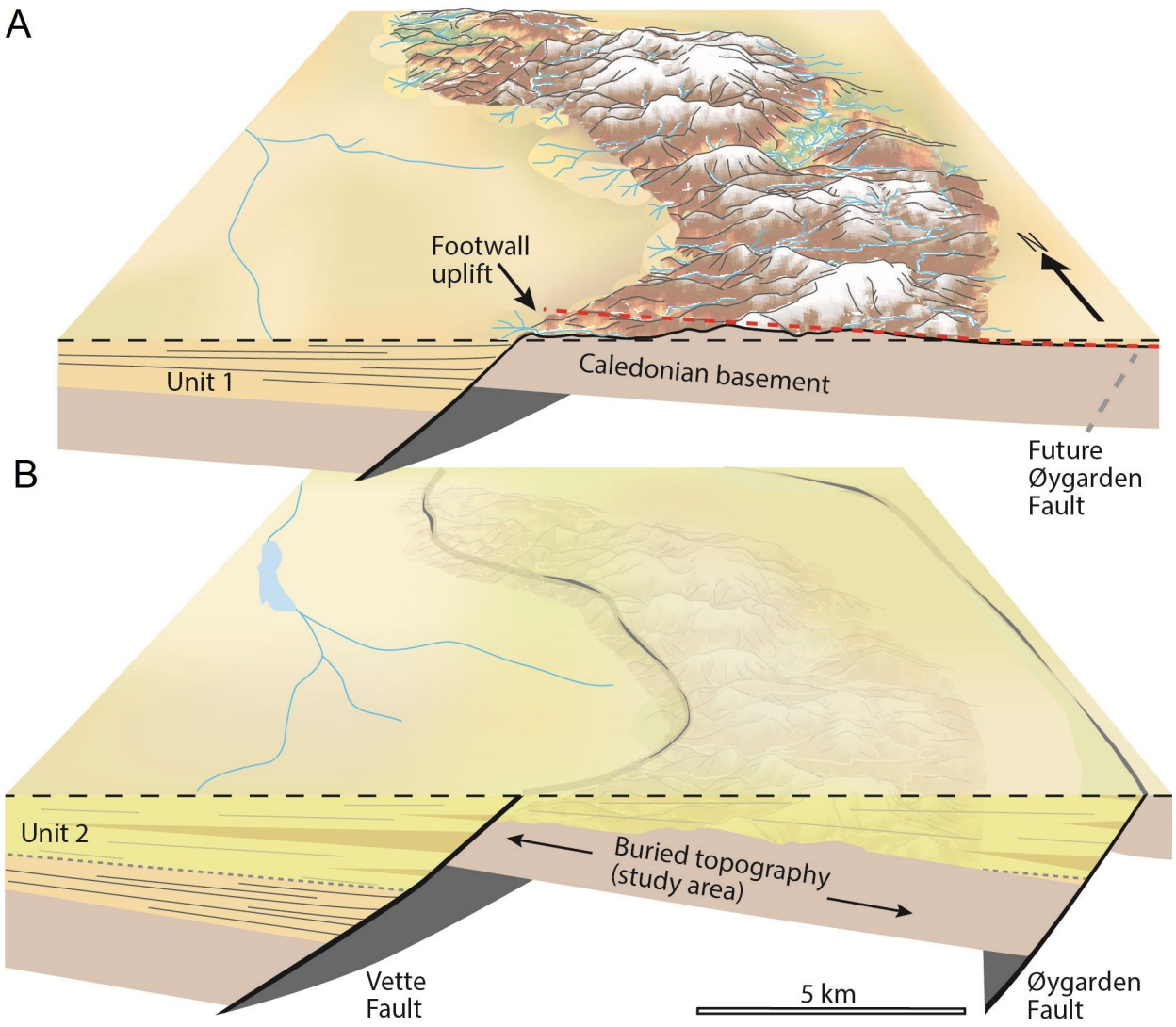

Figure 11: 3D diagram illustrating landscape evolution at the onset of rifting. **A** Landscape development at the onset of rifting in the northern North Sea, when the young Vette Fault initiated and Permian-Triassic strata (Unit 1) were being deposited in its immediate hanging wall. Knickpoints creation when segments of the Vette Fault were displacing palaeo-streams and rivers as they grew, interacted and built footwall relief. **B** Subsequent subsidence and rapid burial underneath Permian-Triassic strata (Unit 2) leading to landscape preservation.

TABLES

Table 1. Geomorphological data extracted from analyzed drainage network.

Number	River length [km]	Catchment area [km^2]
1	7.44	9.9
2	0.44	0.44
3	1.49	1.76
4	5.49	4.82
5	0.29	0.5
6	20.35	60.02
7	1.94	3.44
8	2.93	5.09
9	6.62	18.27
10	1.00	1.36
11	7.15	13.08
12	0.07	0.23
13	18.41	55.83
14	3.61	4.25
15	1.26	1.72
16	1.04	1.02
17	3.16	5.63
18	2.26	1.73
19	0.31	0.28
20	0.05	0.29
21	0.12	0.17
22	2.51	3.17
23	5.84	5.2
24	9.56	25.03
25	3.08	2.64
26	1.71	1.02

27	0.24	0.47
28	1.81	1.28
29	0.12	0.38
30	2.43	2.93
31	6.06	5.3
32	4.64	3.55
33	0.45	0.47
34	5.17	8.54
35	3.67	8.63
36	5.45	3.64
37	4.79	8.43
38	0.81	0.8
39	0.17	0.2
40	0.42	0.53
41	3.92	3.13
42	3.31	3.15
43	0.70	0.59
44	2.09	0.42
45	0.26	2.71
46	3.21	4.62
47	1.95	1.34
48	14.45	50.7
49	0.05	0.34
50	0.05	0.23
51	3.17	3.38
52	7.63	10.13
53	2.87	3.68
54	1.23	1.04
55	1.92	1.62
56	8.20	23.8

57	0.19	0.23
58	5.48	1.02
59	1.63	0.94
60	3.82	0.58
61	0.63	12.52
62	2.35	0.37
63	0.79	6.31
64	1.87	2.06
65	0.53	0.38
66	0.10	2.57
67	0.66	0.91
68	1.17	0.89

Table 2. Knickpoint migration distance extracted from drainage network. Migration times were calculated with rates from Whittaker and Boulton (2012).

Knickpoints	Height [m]	Downstream area [km^2]	Distance from Vette fault [km]	Migration time [Myrs]	Error [Myrs]
1	158	3.71	6.27	14.31	0.14
2	51	1.89	3.85	12.36	0.12
3	96	3.94	2.75	11.01	0.11
4	59	1.81	3.97	12.48	0.12
5	85	11.02	2.69	10.92	0.11
6	52	4.27	6.64	14.54	0.15
7	108	2.91	4.13	12.64	0.13
8	50	0.28	3.41	11.87	0.12
9	56	1.33	1.07	7.18	0.07
10	60	0.05	2.31	10.31	0.10
11	64	5.90	0.44	3.65	0.04
12	75	1.90	4.86	13.29	0.13
13	45	5.95	2.76	11.02	0.11

14	89	0.62	4.88	13.31	0.13
15	74	2.84	1.57	8.78	0.09
16	55	14.37	3.37	11.83	0.12
17	49	6.12	7.58	15.07	0.15
18	65	0.92	4.95	13.36	0.13
19	50	25.00	1.92	9.57	0.10
20	73	7.89	10.00	16.18	0.16
21	59	9.67	5.62	13.87	0.14
22	48	2.32	6.22	14.28	0.14
23	72	1.86	3.05	11.42	0.11
24	45	4.54	2.73	10.98	0.11
25	58	0.68	4.26	12.76	0.13
26	54	14.61	1.64	8.96	0.09
27	48	4.73	7.64	15.10	0.15
28	46	0.00	4.35	12.85	0.13